OPEN ACCESS
IOP Publishing
Superconductor Science and Technology
Supercond. Sci. Technol. **35** (2022) 125003 (11pp)
https://doi.org/10.1088/1361-6668/ac9c99

Reverse coating technique for the production of Nb thin films on copper for superconducting radio-frequency applications

D Fonnesu[1,*], A Baris[1], S Calatroni[1], L Lain Amador[1], S Pfeiffer[1], G Rosaz[1], M Bonura[2] and C Senatore[2]

[1] CERN European Organization for Nuclear Research, Geneva, Switzerland
[2] Department of Quantum Matter Physics, University of Geneva, Geneva, Switzerland

E-mail: dorothea.fonnesu@cern.ch

Received 14 July 2022, revised 5 October 2022
Accepted for publication 21 October 2022
Published 3 November 2022

Abstract

In the framework of the Future Circular Collider Study, the development of thin-film coated superconducting radio-frequency copper cavities capable of providing higher accelerating fields (10–20 MV m^{-1} against 5 MV m^{-1} for the Large Hadron Collider) represents a major challenge. The method investigated here for the production of seamless niobium-coated copper cavities is based on the electroforming of the copper structure around a sacrificial aluminium mandrel that is pre-coated with a niobium thin film. The first feasibility study, applied to a flat aluminium disk mandrel, is presented. Protective precautions are taken towards the functional niobium film during the production process and it is shown that this technique can deliver well performing niobium films on a seamless copper substrate. This way, the non-trivial chemical treatments foreseen by the standard procedures (e.g. SUBU, EP) for the preparation of the copper surface to achieve the proper adhesion of the niobium layer are also avoided. The only major chemical treatment involved in the reverse-coating method is represented by the chemical dissolution of the aluminium mandrel, which has the advantage of not affecting the copper substrate and therefore the copper-niobium interface.

Keywords: Nb, copper, thin films, SRF, bipolar-HiPIMS, FCC, seamless cavities

(Some figures may appear in colour only in the online journal)

1. Introduction

The performance of niobium-coated copper superconducting radio-frequency (SRF) cavities is known to be closely related to the quality of the substrate [1]. While parameters, such as surface roughness can be optimised to a certain degree, the presence of seams and welds cannot be completely avoided with standard cavity fabrication methods [2–6]. A possible way to avoid their presence is offered by the production of copper cavities via electroforming around a sacrificial aluminium mandrel, whose shape and size emulate the ones desired for the final cavity. The idea stems from the original study for the production of non-evaporable getter (NEG) coated, small diameter beam vacuum chambers [7, 8]. The process, addressed as the 'reverse coating technique' [7], consists of forming an aluminium pipe mold (generically addressed as *mandrel*) to which the NEG layer is first coated on the outer wall, and

* Author to whom any correspondence should be addressed.

subsequently of coating a copper layer on top of the NEG film for good adherence of the final copper pipe-structure, which is electroplated (more precisely: electro*formed*) on it. The aluminium mandrel which is left inside is then chemically etched to obtain the final copper pipe having the NEG coating integrated onto the inner walls. The electroforming technique has already been shown to deliver cavities whose copper final properties are comparable to oxygen-free electronic (OFE) grade bulk copper [9, 10], and whose inner surface mirrors the mandrel finish. Once the quality of the electroformed copper cavity structure has reached a satisfying level, the next step is to study the possibility of reproducing the process by also integrating the functional superconducting (SC) layer. In addition to the production of seamless niobium-coated copper cavities, a successful outcome of this process would lead to better adherence, with respect to their counterparts produced according to the standard methods, of the SC film to the copper substrate and make the chemical treatment of the substrate in preparation to the coating no longer needed, as the substrate is directly formed on the film itself.

In this paper, a conceptual study of the applicability of the reverse coating technique to the production of niobium-coated copper SRF cavities is presented. The same production chain developed for NEG-coated vacuum chambers [8] is reproduced for a simple mandrel, such as a flat aluminium disk. The main process is repeated twice: in the first case, the niobium layer is coated directly on the aluminium disk, while in the second case a copper layer is coated on the aluminium, prior to the deposition of the niobium film, for later protection of the niobium from possible damage caused by the final chemical removal of the mandrel. The process for the production of the disks from which the control and test samples are extracted is described in section 2. The characterisation techniques employed to assess the morphology and superconducting quality of the niobium layer at every production step are presented in section 3. The results of the characterisation are presented in section 4. Finally, the next steps are discussed in section 5, including the future challenges.

2. Sample preparation

Two sets of samples where produced for this study: the control set and the reverse-coated set. The control samples, consisting of niobium-coated aluminium substrates, served as a check for the reverse-coated samples. The reverse-coated samples are produced by electroforming copper on a sacrificial aluminium mandrel, which has been pre-coated with a niobium thin film. The process consists of the following essential steps:

(a) manufacturing of the aluminium mandrel;
(b) niobium coating of the aluminium mandrel;
(c) copper coating on top of the niobium layer, to improve the adhesion of the electroplated copper layer;
(d) electroforming of the final copper structure on the coated copper layer;

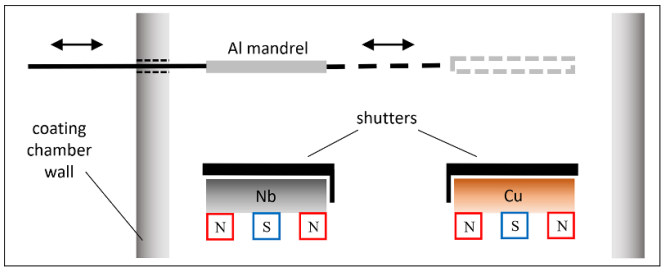

Figure 1. Readapted [8] schematics of the sputtering system used for the coating of the mandrels. The aluminium mandrel is mounted on a translation ultra-high vacuum (UHV) manipulator which allows its position to be adjusted without venting the system. The targets, niobium (left) and copper (right), are depicted with their magnet arrays providing the magnetron field. The shutters cover the targets when not in use.

(e) chemical etching of the aluminium mandrel to obtain the final copper structure with internal niobium coating.

The next subsections provide the details about each step.

2.1. Mandrel manufacturing

In this study, the sacrificial mandrel is represented by a 150 mm diameter and 1.5 mm thick flat aluminium disk. The disks were machined in order to obtain a constant surface roughness (R_a) of 0.3 μm and degreased with a commercial detergent solution (60 °C, 30 min). The study was repeated identically with commercially pure aluminium (AW-1050, 99.5% pure) and with an alloy (AW-6082) as base material with the aim of evaluating the potential impact of impurities originating from the mandrel on the final niobium layer. Two disks were prepared for each aluminium type: one for the control samples and one for the reverse-coated samples. For the control samples, a total amount of six substrates of size $11 \times 35 \times 1.5\,\text{mm}^3$ were cut from the aluminium disks (three per aluminium type) prior to the niobium coating.

2.2. Coating of niobium and copper

The coating chamber is equipped with both the niobium and copper cathodes. The substrate/disk holder is placed at the extremity of a translation ultra-high vacuum manipulator, as shown in figure 1, so that the disk can be moved from the position on top of the niobium cathode to the one on top of the copper cathode (and vice versa) without the need to open the chamber. Thanks to this system, the niobium and copper films can be coated consecutively without venting the system in between, hence avoiding the risk of contamination due to contact with air. Before the coatings, the bakeout of the system was performed at 120 °C for 24 h. During the coatings, the equilibrium temperature reached by the system is 150 °C. All the coatings in this study were performed via the physical vapour deposition (PVD) method known as Bipolar High Power Impulse Magnetron Sputtering (Bipolar-HiPIMS)

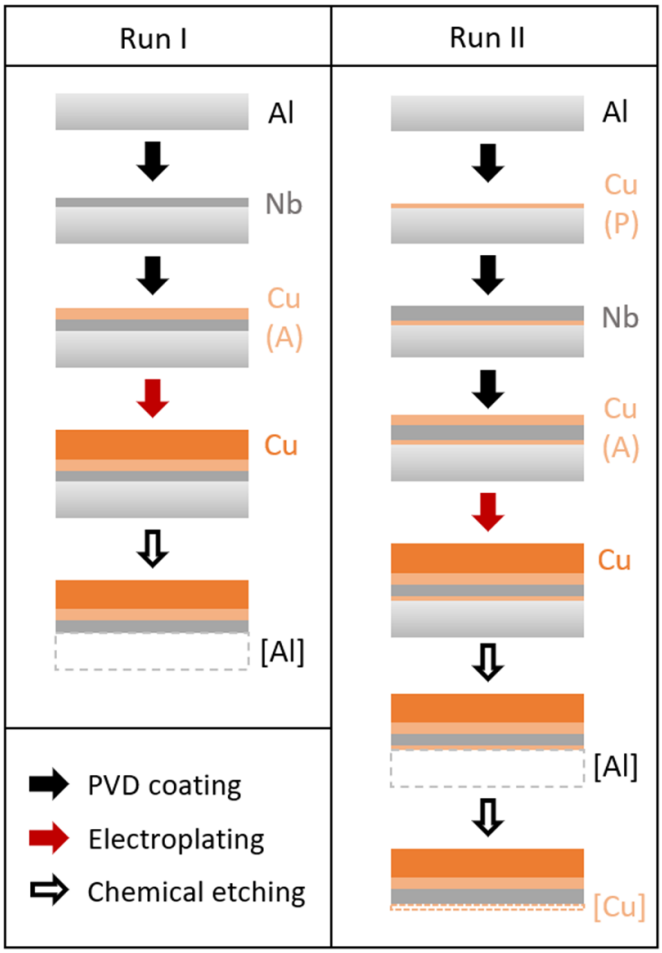

Figure 2. Schematics of the reverse coating technique steps for the case without a copper protective layer (Run I) and with copper protective layer (Run II). The etched layers are indicated in dashed contours and labelled in square brackets.

[11–13]. This technique has been shown to provide denser niobium films on copper substrate than the consolidated Direct Current Magnetron Sputtering technique, and is particularly suitable for coating surfaces at grazing incidence angles with respect to the direction of motion of the sputtered impinging ions [11, 14, 15]. Such properties need to be taken into account for the future application to the production of SRF resonant cavities [13], for which they represent an advantage due to the complex geometries involved.

The control samples were coated first. A 1 μm thick niobium film was deposited on the aluminium substrates and analysed in order to establish a custom coating recipe and a reference to the structural and superconducting properties expected for niobium films deposited on aluminium via Bipolar-HiPIMS.

To produce the reverse-coated samples two different approaches were applied, which are schematically represented in figure 2. In the first case (Run I), a 1 μm niobium film was deposited directly on the aluminium mandrel. In the second case (Run II), a 1 μm thick copper layer (addressed later on as protective layer (P)) is deposited on the aluminium mandrel

Table 1. Coating parameters for the deposition of the niobium film and copper adhesion film (A) in Run I and Run II, and for the deposition of the copper protective film (P) in Run II. All the coatings were performed in krypton atmosphere. MP and PP stand for main pulse and positive pulse respectively.

	Material		
Coating parameter	Nb	Cu (A)	Cu (P)
P_{Kr} (mbar)	1.4×10^{-3}	1.4×10^{-3}	1.2×10^{-3}
MP amplitude (V)	−500	−760	−760
MP duration (μs)	50	50	50
Peak current (A)	33	22	20
Peak power (kW)	15	15	14
Average power (W)	280	350	310
PP amplitude (V)	130	130	130
PP duration (μs)	200	200	200
Delay (μs)	1	1	1
Frequency (kHz)	1	1	1
t_{coat} (min)	240	120	90

prior to the niobium (i.e. between the aluminium and the 1 μm niobium layer deposited later on). In both cases, a 3 μm thick copper layer was then deposited on top of the niobium film, to serve as adhesion layer (A) for the electroforming of the final copper structure. The parameters of the sputtering process are summarised in table 1.

2.3. Electroforming of copper

After the coating, in order to electroform the final copper structure, the mandrels were assembled on a special support which provides an electrical contact and, at the same time, protects the mandrel from the undesired deposition of copper on the rear side. The electroplating of a 0.5 mm thick copper layer was performed in a copper sulphate ($CuSO_4\,5\,H_2O$) sulfuric acid (H_2SO_4) bath with the presence of a brightener, with an applied current of 200 A m^{-2} for a duration of 20 h. The mandrel before and after the coating phase, and after the copper electroforming (with and without support) can be seen in figure 3.

2.4. Etching of mandrel

Finally, the mandrels were dismounted from the support for the electroplating and samples of size $10 \times 35 \times 1.5\,\text{mm}^3$ were cut from them to proceed with the characterisation, which was done both with the aluminium mandrel still present (i.e. before etching) and after the aluminium mandrel removal. The chemical etching of the aluminium mandrel was performed in a sodium hydroxide bath (NaOH 5×10^3 mol m^{-3}, room temperature). For the samples having the protective copper layer on top of the niobium, ammonium persulfate ($(NH_4)_2S_2O_8$ 150 g l^{-1}, room temperature) was also used to chemically etch the protective copper layer after the aluminium removal. The etched layers are indicated enclosed in square brackets (e.g. [Al], [Cu]) in figure 2 and in the text to follow.

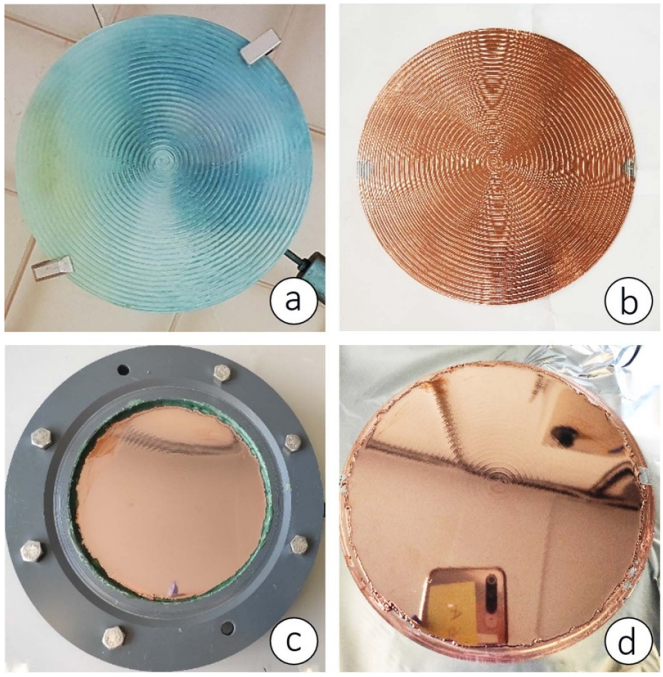

Figure 3. AW-1050 aluminium mandrel mounted inside the coating chamber before the coating of the niobium and copper adhesion films (a), after the coating (b) and after the electroplating of the final copper structure, still mounted on the special support for the electroplating (c) and without the support (d).

3. Sample characterization

After the production of every sample batch (control samples, reverse-coated samples without and with copper protective layer), the morphology and superconducting performance of the niobium films were evaluated. At this stage of the study, it was important to assess the potential of the reverse coating technique to deliver suitable niobium films for an SRF end-use, exhibiting satisfying purity levels and regular morphology, free of porosities. Hence the characterisation phase focused on the measurement of the critical temperature (T_c) and on the imaging of the sample cross section. In the case of the reverse-coated samples, the inductive test was performed before and after the mandrel removal and the results are presented together for comparison. Based on the outcome, the characterisation was carried further on with the measurement of the critical current density (J_c) for a selection of samples that showed the best properties. This physical quantity depends on the concentration of pinning centres [16, 17] and therefore provides insight into the amount of structural defects [18] which can be present in the material.

The critical temperature was measured via a contactless, coil-induction setup [11, 19] available at the Central Cryogenic Laboratory at CERN and optimised for the measurement of the critical temperature of superconducting thin films deposited on copper substrate. The measurement system consists of two coaxial coils placed in front of each other. The sample, of standard size $11 \times 35 \times 1\,\text{mm}^3$ is placed between the coils, exposed to a constant helium vapour flow and cooled down below its critical temperature (in case of niobium, the expected critical temperature for the pure bulk material is 9.29 K [20]). Once the sample temperature is stable at 8 K, a low-frequency (21 Hz) sinusoidal magnetic field of constant amplitude is turned on in front of, and perpendicular to the film surface, by exciting the drive (d) coil placed in front of the sample side with the functional layer on it (the niobium film in this case). The magnetic flux density generated at the coil has a value of about 3 mT and decreases to 0.2 mT at the sample surface. By running a temperature ramp up to 10 K it is possible to measure the change in mutual inductance, hence in induced electromotive force, in the pickup (pu) coil placed at the opposite side of the sample. This is due to the change of state, from superconducting (magnetic field is expelled) to normal conducting (magnetic field can cross the film), that the sample undergoes when its critical temperature is crossed, which results in an increased magnetic flux density across the pickup coil. T_c is extracted as the temperature corresponding to the half-height of the step-like amplitude of this voltage drop, which is later on referred to as A_{pu}. The width of the transition curve, defined here as $\Delta T_c = T^{90\%} - T^{10\%}$, is also indicative of the sample purity. The cross section of the films was prepared via focused ion beam and analysed via scanning electron microscopy (FIB-SEM). The used equipment is located at the Materials and Metrology laboratory at CERN and consists of a Zeiss Crossbeam 540 SEM equipped with FIB. The imaging is performed by InLens and Secondary Electron Secondary Ion detectors. In order to perform the milling needed for inspection of the sample cross section, a protective platinum layer ($20 \times 2 \times 1\,\mu\text{m}^3$) is deposited with an ion beam current of 300 pA and accelerating voltage of 30 kV. A $20 \times 10 \times 4\,\mu\text{m}^3$ sample volume was then coarsely milled with an ion beam current of 3 nA and accelerating voltage of 30 kV. Prior to imaging, the cross-sectional surface was smoothened with an ion beam current of 300 pA and an accelerating voltage of 30 kV. The SEM imaging of the sample cross sections was performed at an accelerating voltage of 3 kV. Thanks to this technique it was also possible to infer the average film thickness.

The critical current density of the films was measured at the University of Geneva by means of a Superconducting Quantum Interference Device (SQUID) vibrating sample magnetometer (VSM) by Quantum Design. The device is equipped with a superconducting coil able to generate magnetic fields up to 7 T and to cover the temperature range 1.8 K–400 K. For these measurements, the standard sample size is $3 \times 3\,\text{mm}^2$ with variable thickness: 1.5 mm for the aluminium substrate and 0.5 mm for the copper substrate for this study case. By measuring isothermal loops of the magnetic moment $m(B)$ in the field range −7 T–7 T it is possible to calculate J_c in the frame of the Bean critical state model using the equation $J_c(T,B) = \frac{2\Delta m(T,B)}{Vt}$, which is valid for a slab geometry in parallel magnetic field, where $\Delta m(T,B)$ is given by the separation of the branches of the magnetic moment loop $m(B)$ measured with opposite field sweep directions at a given temperature T, and Vt is the product of the volume V of the superconducting sample and its thickness t. The temperature values at which the

Table 2. Summary of the results of the characterisation measurements of the control and reverse-coated (Run I, Run II) samples. The material removed by chemical etching is indicated inside square brackets in the sample label. The measurements which were not performed are indicated by '—' while the measurements which were not conclusive are indicated by 'x'.

	Characterisation results				
	T_c (K)	ΔT_c (K)	d (μm)	$J_c(4\,K, 0.2\,T)$ (MA mm^{-2})	$B_{c2}(4\,K)$ (T)
Control samples					
AW-1050	9.32	0.07	1	2.5	1.25
AW-6082	9.33	0.07	1	0.29	0.95
Run I					
Cu–Nb–Al	9.35	0.11	—	—	—
Cu–Nb–[Al]	x	x	1	—	—
Run II					
Cu–Nb–Cu–Al	9.34	0.04	—	—	—
Cu–Nb–Cu–[Al]	9.34	0.06	—	—	—
Cu–Nb–[Cu]–[Al]	9.33	0.05	1	0.16	0.95

loops $m(B)$ are measured range from 2.5 K to 9 K. This investigation also allows the estimation of the upper critical field B_{c2}, defined here as the intersection point of $J_c(B)$ with the $J_c = 0$ line.

4. Results and discussion

In the following sections the outcome of the characterisation of the Nb–Al control samples, the Cu–Nb–[Al] samples from Run I and the Cu–Nb–[Cu]–[Al] samples from Run II is presented and discussed in detail for each case. The results of the characterisation measurements are summarised in table 2 for all the samples.

4.1. Nb–Al control samples

The niobium control samples deposited on the aluminium substrates were analysed first, in order to assess the quality of the coating recipe and the features presented by the film on the aluminium substrate. In figure 4 the substrates are shown mounted on the disk holder before (a) and after (b) the niobium coating. Aluminium AW-1050 was used for samples 1, 2 and 3, while AW-6082 was used for samples A, B and C. The shape of the superconducting transition curves obtained with the inductive measurement is shown in figure 5 and does not present any unusual feature, suggesting the absence of anomalies in the control films that could affect the superconducting state and the passage to the normal state. A higher value of T_c is normally observed for niobium films with respect to their bulk counterparts due to residual compressive stress induced during the sputtering process, and is expected to decrease with increasing sample thickness [21]. The measured values are nevertheless comparable to T_c of the pure bulk material [20], indicating a good level of purity of the control films. In addition to this, it is possible to observe that films deposited on aluminium alloys of different purity show the same T_c, suggesting that the purity of the mandrel employed in the reverse coating process is not expected to be relevant for the purity of the functional niobium layer. The transition width ΔT_c is comparable to what is observed from typical inductive measurements of bulk niobium [19] ($\Delta T_c \simeq 0.05\,K$), also an indication of a low concentration level of impurities in the samples. The signal produced by the leak field when the samples are in the superconducting phase ($T < T_c$) is the same, as shown by the overlapping signal before the phase transition takes place, and differs towards lower temperatures due to effects of the coating on the sample edges. These effects are object of a later study on Nb_3Sn films deposited via Bipolar-HiPIMS on copper. The shape of the superconducting transition, the presence of additional transition steps at a temperature different from the T_c of the coating on the main face of the sample and irregular (i.e. non-flat) shapes of the superconducting side of the curve are observed when the coating is present on the edges of the sample and disappear when the edge coating is removed. The interpretation of these features is still ongoing and the study [22] yet to be published. The $0.2\,\mu V$ difference between the signals on the normal conducting side of the curve (for $T > T_c$) does not depend on the films but rather on the different composition of the aluminium alloys used as substrate. For temperatures lower than 10 K, an electrical resistivity of $\rho > 0.1\,\mu\Omega\,cm$ has to be expected for the AW-6082 and AW-1050 alloys [23], which results into a minimum skin depth of 3.5 mm for the aluminium substrates at the applied frequency of 21 Hz. Although this is more than a factor 2 larger than the substrate thickness, making it nearly transparent to the magnetic field, the difference in resistivity between the two alloys is such that the eddy currents induced in the aluminium by the magnetic field have higher intensity for the alloy with smaller resistivity (AW-1050). This finally leads to a stronger screening by the eddy currents induced into the AW-1050 substrate than the ones in the AW-6082: the latter are indeed not strong enough to separate the normal conducting signal from the signal induced into the pickup coil without a sample in between the coils (shown in light grey in figure 5), while in the lower resistivity alloy the currents are intense enough to partly screen the magnetic field and separate the signal from the bare-coils one.

The SEM images of the niobium film FIB-milled cross section are shown in figure 6, with the film coated on the

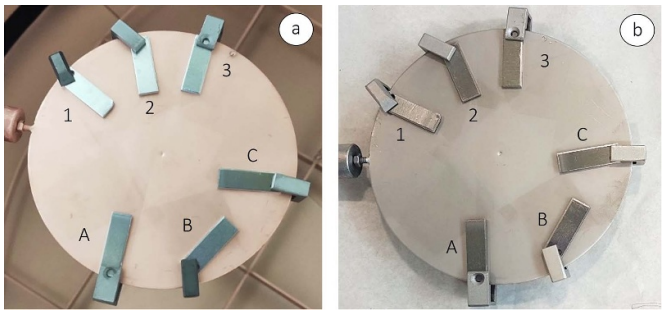

Figure 4. Aluminium substrates mounted on the disk holder before (a) and after (b) the coating of the niobium control film. The AW-1050 substrates are labelled as 1, 2, and 3; the AW-6082 substrates are labelled as A, B, and C.

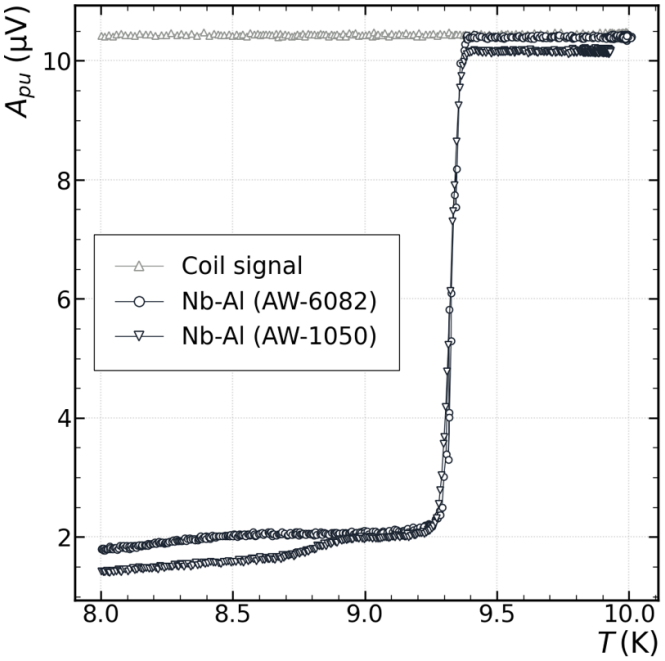

Figure 5. Inductive measurement of the superconducting to normal conducting state transition of the niobium control samples deposited on the AW-6082 (circles) and AW-1050 (triangles) aluminium substrates (black). The bare coil signal is also shown for comparison (triangles, grey). The sample T_c is extracted as the temperature corresponding to the half-height of the transition curve.

AW-6082 substrate shown in figure 6(a) and the one on the AW-1050 substrate in figure 6(b). In both images, the protective platinum layer (Pt) is visible as first layer on top, followed by the niobium film (Nb) below and the aluminium substrate last (Al). Both niobium films appear dense, free of voids and show good adhesion to the substrate. The columnar growth pattern typical of PVD thin films is also visible, with a coarser structure at the substrate interface, this being the first one to be deposited and therefore containing the initially nucleated film grains [24]. The SEM imaging of the film cross section made also possible to infer the average thickness of the niobium layer to be 1 μm along the milled length for both samples.

The critical current density J_c extracted from the $m(T,B)$ loops is shown in figure 7(a) for the film deposited on the AW-6082 substrate and in figure 7(b) for the one deposited on the AW-1050 substrate. The resulting J_c values at $B = 0.2$ T and $T = 4$ K are 0.29 MA mm^{-2} for the sample on the AW-6082 substrate and 2.5 MA mm^{-2} for the sample on the AW-1050 substrate. It is preferable that niobium films produced for SRF application exhibit critical current values which are as low as possible, and these values can be considered satisfying [18] for a niobium film of 1 μm thickness within the scope of this study. However, they still suggest the presence of high density of dislocations in the material [13]. One can also consider further reducing this J_c value especially when compared to currently used state-of-the-art bulk Nb that exhibits critical current density values in the order of 10 kA mm^{-2}[25]. Overall, the control niobium films exhibited good superconducting properties and classic structural features, reason why the same coating recipe was also adopted for the next two coating runs for the production of the reverse-coated samples. In light of the results obtained with the characterisation measurements of the control samples, to avoid redundancy only the results obtained for the samples produced with the AW-1050 aluminium mandrel will be presented and discussed in the next subsections.

4.2. Run I: reverse Cu–Nb samples without Cu protective layer

The inductive measurement of the Run I samples, shown in figure 8, lead to a regular transition curve only for the Cu–Nb–Al (pre-etching) sample, while for the Cu–Nb–[Al] (post-etching) it revealed a poor-to-absent superconducting phase. The fact that the Cu–Nb–Al sample showed a higher value for T_c than the control samples is likely an indication of a higher compressive residual stress level. This can be explained considering that in this case, not only the niobium film suffers from the residual stress caused by the growth process on the aluminium, but it is also constrained by the additional copper layer grown onto it which in turn adds up to the original stress introduced by the first coating. The increased transition width suggests the possibility of larger concentration of impurities with respect to the control samples. The signal for $T > T_c$ is about 1 μV smaller for this sample with respect to the control samples due to the presence of the copper layer. The copper electroformed according to the procedure described in section 2 has been shown to have properties comparable to the OFE-grade copper [10] employed at CERN for the production of SRF cavities. One can assume RRR $\geqslant$ 50 and hence an electrical resistivity $\rho \leqslant 0.03\,\mu\Omega$cm for low temperatures (<10 K). This results in eddy currents which are a factor 3–4 higher in intensity than in the aluminium mandrel and whose effect results into a normal conducting signal, which is about a factor 4 more damped for the reverse coated Cu–Nb–[Al] sample than for the Nb–Al (AW-1050) control sample. The normal conducting signal for the Cu–Nb–Al sample is even lower as the screening effect of the eddy currents generated into the aluminium adds up to the ones in the copper. The Nb–Cu–Al sample also shows, for $T < T_c$, a superconducting screening signal in full agreement with the screening levels

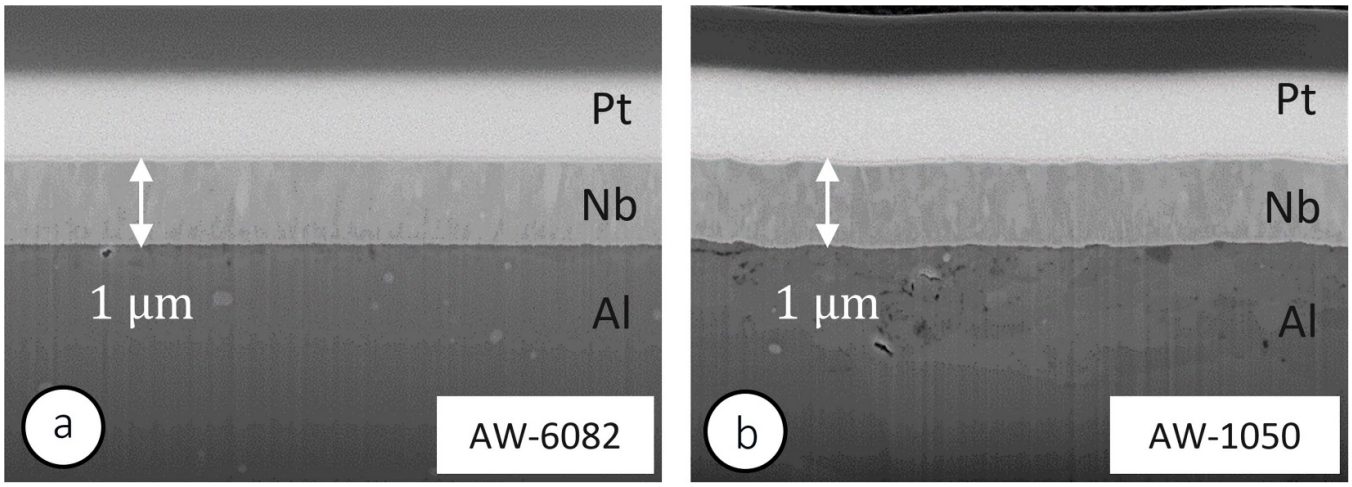

Figure 6. SEM micrographs of the FIB-milled cross section of the niobium control samples. The sample deposited on the AW-6082 substrate is shown in figure (a) and the one deposited on the AW-1050 substrate is shown in figure (b). In both images, the platinum (Pt) protective layer is visible on top, followed by the niobium film (Nb) in the middle and the aluminium substrate (Al) at the bottom. The indicated film thickness of 1 μm also provides the image scaling.

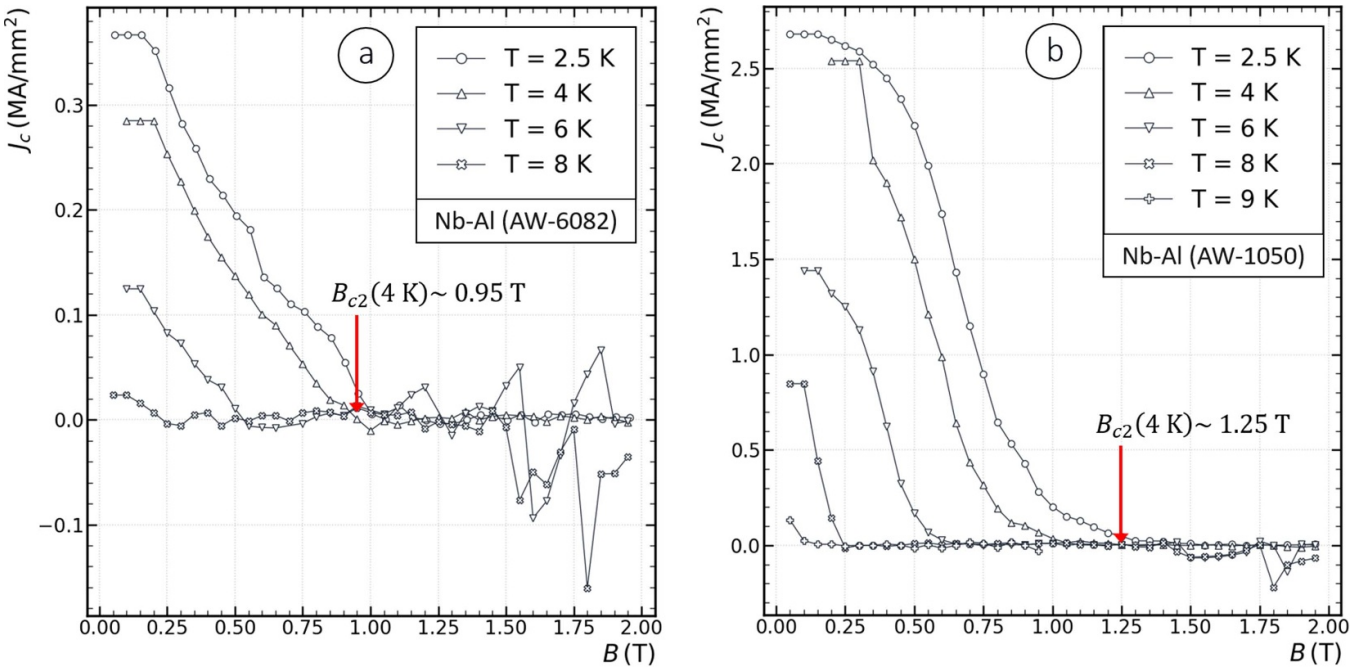

Figure 7. Critical current J_c of the niobium control samples calculated, in the framework of the Bean critical state model, from the VSM-SQUID measured sample magnetic moment loops $m(B)$ at different fixed temperatures. The upper critical field B_{c2} is taken as the field value at which $J_c(4\,\mathrm{K}) = 0$. The curves measured for the sample deposited on the AW-6082 and the AW-1050 substrates are shown in plot (a) and (b) respectively.

observed in the control samples. The fact that after the mandrel removal the niobium sample no longer shows the signs of a superconducting phase (the screening is reduced by a factor ~4, absence of a step-like signal corresponding to the phase transition across T_c) suggested that the chemical etching process applied to remove the aluminium was detrimental to the functional film.

The SEM images of the FIB-milled cross section of two Cu–Nb–[Al] samples are shown in figure 9 and support the interpretation that the observed degraded superconducting performance of the sample is due to the aluminium etching. Figure 9(a) shows the sample also discussed above in the inductive measurements, which was left in the etching solution for as long as the etching process took place (27 h) and removed as soon as it was finished. The main difference observable here with respect to the control film in figure 6 is that the first deposited niobium layer corresponds now to the upper part of the film, i.e. the former interface with the aluminium mandrel. The 3 μm thick coated copper adhesion layer (A) is also visible as the large, columnar band structure below

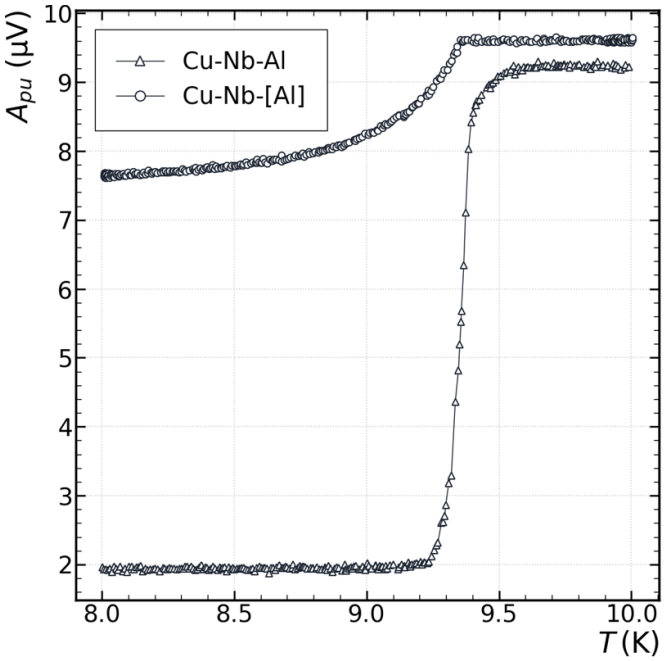

Figure 8. Inductive measurement of the superconducting to normal conducting state transition of the reverse coated Cu–Nb–Al sample (Run I) before (triangles) and after (circles) the etching of the aluminium mandrel. The phase transition in the Cu–Nb–[Al] sample appears degraded by the mandrel removal process.

the niobium layer. Apart from these aspects, the sample does not appear appreciably different from the control samples. Figure 9(b) instead was taken of a sample that was left in the etching solution for 1 h longer after the etching process was finished (28 h). Here the sample appears damaged, with the part exposed to the etching solution being porous and at intervals, detached from the material below. Naturally, niobium is protected by an air-formed oxide layer (Nb_2O_5) which is enough to prevent corrosion by the sodium hydroxide in short exposure times. However, open-circuit potential (OCP) measurements versus exposure time of niobium in NaOH solution (at different concentrations and temperatures) have shown that the OCP decreases with time, indicating the dissolution of the oxide layer and the activation of the underlying niobium surface [26]. In the case of the Cu–Nb–[Al] sample, the niobium film was deposited on aluminium and never exposed to air, which prevented the formation of the protective oxide layer on its surface. As soon as the aluminium layer was completely removed, two main processes are likely to have taken place resulting in the degradation of the niobium film: for the sample that was removed from the solution right at the end of the aluminium etching, the hydrogen produced in the reaction ($2Al_{(s)} + 2NaOH_{(aq)} + 2H_2O_{(aq)} \rightarrow 2NaAlO_{2(aq)} + 3H_{2(g)}$) started diffusing into the niobium; in addition to this, for the sample that was left in the solution for 1 h longer than the end of the etching of the aluminium, the hydrogen diffused into the niobium creating enough defects to promote the propagation of the reaction from the surface into the film. It must be made clear that the presence of the NaOH in the solution is secondary to the initiation of the corrosion of niobium. In fact, the cathodic reaction dominating on metallic niobium under the conditions described by Robin [26] is: $2H_2O + 2e^- \rightarrow H_2 + 2OH^-$ due to which niobium, at OCP, starts dissolving under the effect of the hydroxyl ions. The soluble niobates which form as a result of this process will in turn precipitate as sodium niobium oxide hydrates when their solubility limit is reached, thanks to the presence of the NaOH. Considering these results, it was decided not to proceed with the measurement of the sample critical current, as it would have not provided additional insight on the interpretation of the effects of the mandrel etching on the niobium film, with respect to what was already obtained from the inductive and SEM measurements. Instead the choice was made to modify the manufacturing process in order to add a protective layer as presented in the section 2.

4.3. Run II: reverse Cu–Nb samples with Cu protective layer

The results of the inductive measurements performed for the samples from Run II are presented in figure 10. For these samples a copper protective layer (indicated as (P) in figure 2) was deposited on the aluminium mandrel prior to the deposition of the niobium film, differently from Run I in which the niobium film was deposited directly on the mandrel. At every production step (i.e. for Cu–Nb–Cu–Al, the sample as-deposited; Cu–Nb–Cu–[Al], after the etching of the mandrel; Cu–Nb–[Cu]–[Al], after the etching of the copper protective layer (P)) the niobium film shows a regular superconducting transition curve, which suggests the production process to be free from steps that can negatively affect the superconducting properties. All the measurements show values of the critical temperature T_c in accordance with the values measured for the control samples. The superconducting transition appears sharp for all the samples, with transition width ΔT_c values in the range 0.04–0.06 K which are smaller than what observed for the control samples, $\Delta T_c = 0.07$ K. The normal conducting signal (for $T > T_c$) for the Cu–Nb–Cu–Al sample is 0.5 μV smaller than the signal observed for the Cu–Nb–Cu–[Al] and Cu–Nb–[Cu]–[Al] samples, due to the screening effect introduced by the eddy currents in the aluminium layer, as previously explained in the discussion of the results from Run I. The signal for the Cu–Nb–Cu–[Al] and Cu–Nb–[Cu]–[Al] samples overlaps as the copper protective (P) layer is not thick enough (1 μm) for the eddy currents to result in a detectable screening effect. The superconducting screening signal (for $T < T_c$) for all three samples is consistent with what observed for the control samples and for the samples from Run I. The fact that the signal for $T < T_c$ remains flat for the Cu–Nb–Cu–Al sample while it presents a positive slope for the etched samples suggests that the sides of the niobium film (which are exposed to the etching solution along the cut sample edges) were damaged, facilitating early penetration of magnetic flux lines into the sample as the temperature increased towards T_c. The slope remains unchanged from the Cu–Nb–Cu–[Al] sample to the Cu–Nb–[Cu]–[Al] sample, also suggesting that the mandrel etching process affected the exposed parts of the niobium film (introducing the slope), rather than the etching of the copper protective layer, after which the shape of the transition curve remains the same.

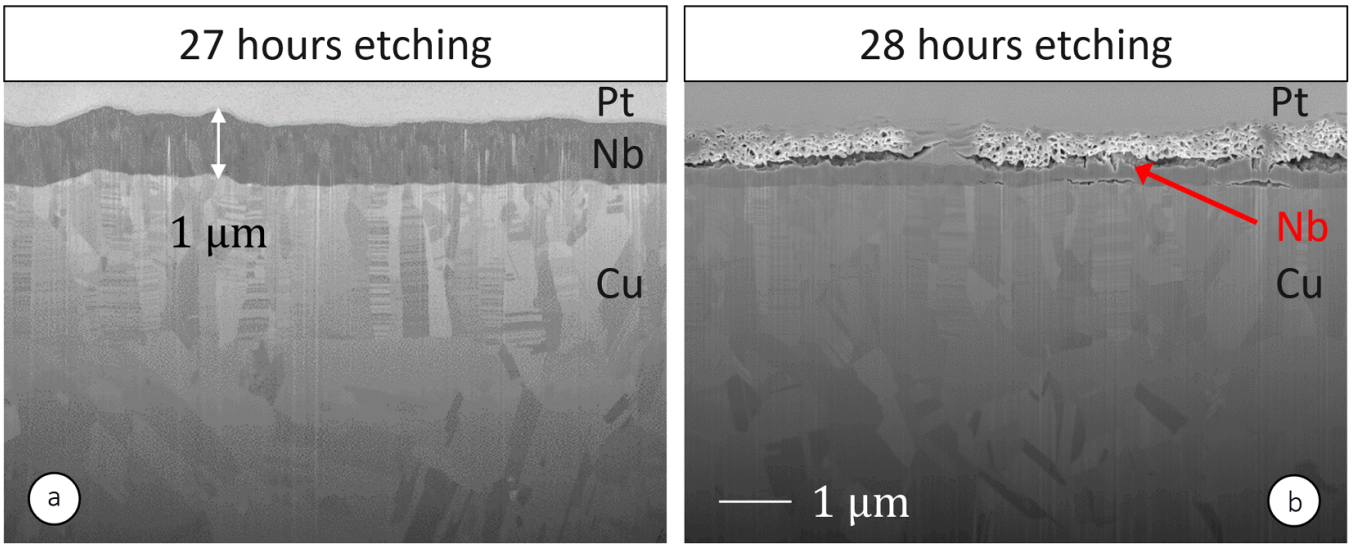

Figure 9. SEM micrographs of the FIB-milled cross section of the reverse coated Cu–Nb–[Al] samples. In figure (a) is the sample etched for 27 h, time needed for the complete removal of the aluminium mandrel. In figure (b), the sample etched for 28 h, one hour longer than the needed time, showing the signs of damage from exposure to the etching solution. In both images, the platinum (Pt) protective layer is visible on top, followed by the niobium film (Nb) in the middle and the copper (Cu) at the bottom.

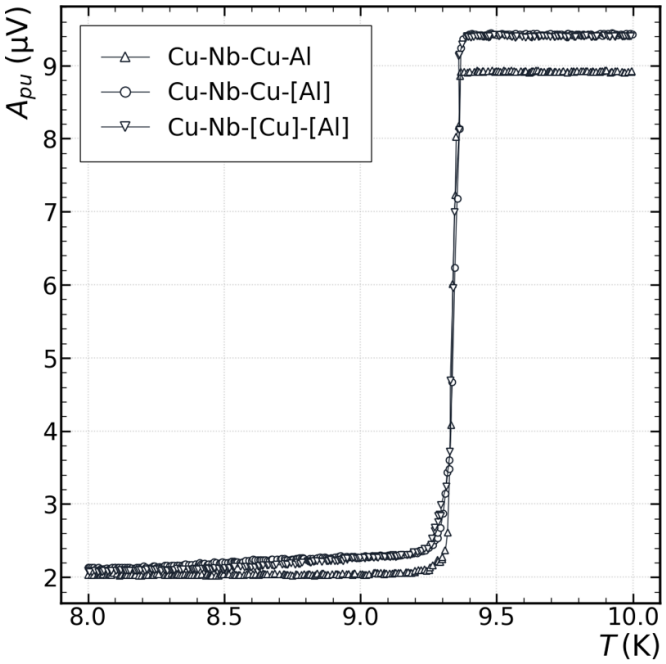

Figure 10. Inductive measurement of the superconducting to normal conducting state transition of the reverse coated Cu–Nb–Cu–Al sample (Run II) before any etching (up triangles), after the etching of the aluminium mandrel (circles) and after the etching of the copper protective layer (down triangles). The etching stages do not affect the phase transition, except for causing early field penetration from the film edge which was exposed to the mandrel etching solution. This is visible from the positive slope shown by the etched samples for $T < T_c$.

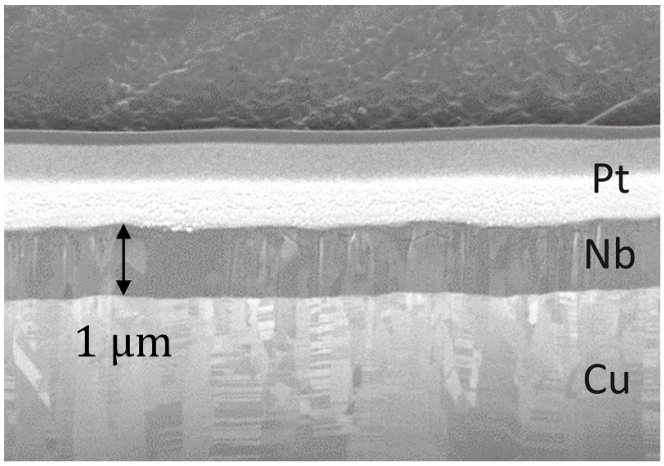

Figure 11. SEM micrographs of the FIB-milled cross section of the reverse coated Cu–Nb–[Cu]–[Al] sample. The platinum (Pt) protective layer is visible on top, followed by the niobium film (Nb) in the middle and the copper (Cu) at the bottom.

The effectiveness of the copper protective layer (P) is confirmed by the SEM images of the FIB-milled cross section of the Cu–Nb–[Cu]–[Al] sample shown in figure 11, where the niobium film (Nb) is visible between the platinum (Pt) and the copper (Cu) layers. Other than the uppermost part of the film (the first one to be deposited), which might present a different nucleation pattern with respect to the niobium films deposited in Run I, which were deposited on aluminium and not on copper, there are no structural differences that can be observed between these samples and the ones coated previously. The film is dense, in good adhesion with the copper layer and overall appears healthy.

The VSM-SQUID measurement of the critical current density J_c of the Cu–Nb–[Cu]–[Al] sample, from which the upper critical field B_{c2} is also extracted, is shown in figure 12. At a temperature of 4 K the low field value of J_c is about a factor 8.7, and the value for B_{c2} a factor 1.2, smaller than the average of what was measured for the control samples.

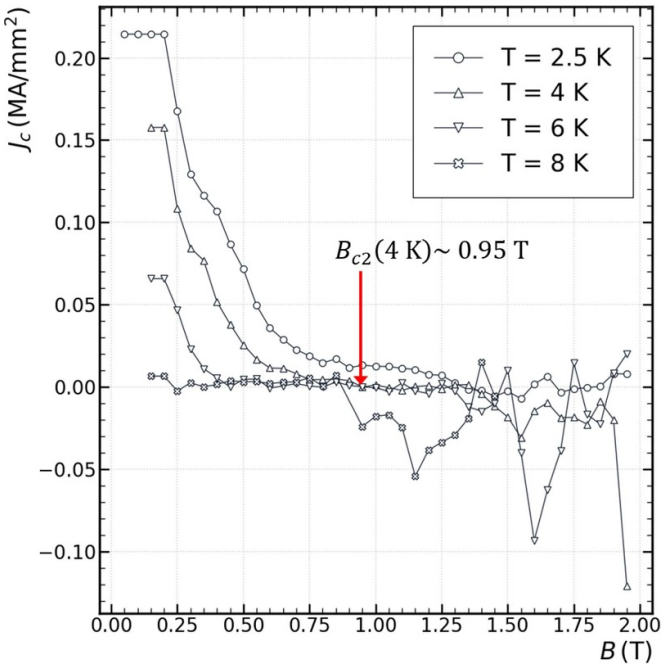

Figure 12. Critical current J_c of the niobium control samples calculated, in the framework of the Bean critical state model, from the VSM-SQUID measured sample magnetic moment loops $m(B)$ at different fixed temperatures. The upper critical field B_{c2} is taken as the field value at which $J_c(4\,\mathrm{K}) = 0$.

As J_c and B_{c2} are both expected to increase with the sample disorder [18], these measurements prove that the procedure established in Run II for the production of the reverse-coated samples can provide niobium films whose performance is comparable (if not improved) to the control niobium samples deposited on the mandrel.

5. Conclusion

The process conceived for the production of NEG-coated vacuum chambers was applied for the first time to the case of niobium-coated copper cavities. Here a conceptual study of the process is presented, for which the steps were reproduced for a simpler structure than a resonant cavity, i.e. a flat aluminium disk. While the quality of the copper substrate produced in this way was previously assessed [10], this study shows that the niobium film can withstand the formation process and that the final quality is satisfying in the context of the performed characterization. In Run I the niobium film was deposited directly on the aluminium mandrel and the final etching for the mandrel removal turned out to be detrimental to the niobium layer. In Run II a copper layer was coated on the aluminium mandrel prior to the deposition of the niobium film, which successfully protected the niobium from the etching of the aluminium mandrel and could be etched itself with no consequences on the niobium. The final niobium layer showed a regular appearance from the SEM scans and the capability to form a good superconducting phase via inductive measurement of T_c and VSM-SQUID measurements of J_c. The fact that the niobium film was deposited on the copper protective layer (P) instead of on aluminium might have even improved the film quality with respect to the control samples. Two advantages are to be underlined about the reverse coating technique with respect to standard fabrication methods: it does not only allow for the production of seamless cavities, but also removes the surface chemistry (needed to prepare the substrate for the coating of the functional film) from the list of mandatory production stages, from which the quality of the film can depend strongly. The next natural step in the feasibility study would be the assessment of the radio-frequency (RF) performance of the samples, but the way to proceed still has to be defined. The manufacturing of a sample suitable for quadrupole resonator [13] testing is not feasible. Loading a flat sample inside a high-frequency test resonator, or directly manufacturing a higher frequency, elliptical cavity (e.g. 1.3 GHz) will be considered as options. With regard to this, the treatment of the mandrel surface, which in principle could simply be machined with mirror-like surface finish, and the related consequences on the RF behaviour of the film are yet to be studied. Whether and how this will have an impact on the RF performance is currently an open question.

Data availability statement

The data that support the findings of this study are available upon reasonable request from the authors.

Acknowledgments

The authors wish to thank their colleagues at the CERN Cryo-Lab: L Dufay-Chanat, T Koettig, S Prunet, A Vacca for the technical support and L Ferreira from the CERN Vacuum, Surfaces and Chemistry group for his chemistry expertise.

This research was supported by EASITrain—European Advanced Superconductivity Innovation and Training. This Marie Sklodowska–Curie Action (MSCA) Innovative Training Network (ITN) has received funding from the European Union's H2020 Framework Programme under Grant Agreement No. 764879.

ORCID iDs

D Fonnesu https://orcid.org/0000-0002-5430-948X
S Calatroni https://orcid.org/0000-0002-2769-8029
G Rosaz https://orcid.org/0000-0001-5987-128X
M Bonura https://orcid.org/0000-0002-8512-0989
C Senatore https://orcid.org/0000-0002-9191-5016

References

[1] Benvenuti C, Calatroni S, Campisi I E, Darriulat P, Peck M A, Russo R and Valente A-M 1999 *Physica* C **316** 153–88
[2] Palmieri V 1998 Review of Fabrication of Superconducting Cavity Structures *LINAC98-XIX International Linear Accelerator Conf.* (*Chicago, Illinois, USA, 23–28 August 1998*) (available at: http://accelconf.web.cern.ch/l98/linac98.html)

[3] Palmieri V, Preciso R, Ruzinov V L and Stark S Y 1993 *Proc. 6th Int. Workshop On RF Superconductivity*
[4] Singer W 2017 *Supercond. Sci. Technol.* **30** 033001
[5] Croteau J-F, Robin G, Cantergiani E, Atieh S, Jacques N, Mazars G and Martiny M 2021 *J. Eng. Mater. Technol.* **144** 021004
[6] Benvenuti C, Circelli N and Hauer M 1998 *Appl. Phys. Lett.* **45** 583
[7] Lain Amador L, Chiggiato P, Ferreira L M A, Nistor V, Perez Fontenla A T, Taborelli M, Vollenberg W, Doche M-L and Hihn J-Y 2018 *J. Vac. Sci. Technol.* A **36** 021601
[8] Lain Amador L 2019 Production of ultra-high-vacuum chambers with integrated getter thin-film coatings by electroforming *Doctoral Dissertation* U. Bourgogne Franche-Comte
[9] Rosaz G J 2019 *Conf. Talk (SRF2019 FRCAB2)*
[10] Lain Amador L, Chiggiato P, Ferreira L M A, Garcia-Tabares E, Koettig T, Meyer M S, Perez-Fontenla A T, Puthran K, Rosaz G and Taborelli M 2021 *Phys. Rev. Accel. Beams* **24** 082002
[11] Avino F, Avino F, Fonnesu D, Koettig T, Bonura M, Senatore C, Perez Fontenla A T, Sublet A and Taborelli M 2020 *Thin Solid Films* **706** 138058
[12] Avino F, Manke F, Richard T and Sublet A 2021 *Plasma Sources Sci. Technol.* **30** 115015
[13] Arzeo M, Avino F, Pfeiffer S, Rosaz G, Taborelli M, Vega-Cid L and Venturini-Delsolaro W 2022 *Supercond. Sci. Technol.* **35** 054008
[14] Alami J, Persson P O Å, Music D, Gudmundsson J T, Bohlmark J and Helmersson U 2005 *J. Vac. Sci. Technol.* A **23** 278–80
[15] Nakano T, Hirukawa N, Saeki S and Baba S 2013 *Vacuum* **87** 109–13
[16] Matsushita T 2007 *Flux Pinning in Superconductors* (New York: Springer)
[17] Antoine C 2019 *Phys. Rev. Accel. Beams* **22** 034801
[18] Casalbuoni S, Knabbe E A, Kötzler J, Lilje L, von Sawilski L, Schmüser P and Steffen B 2005 *Nucl. Instrum. Methods Phys. Res.* A **538** 45–64
[19] Fonnesu D *et al* 2022 *Proc. SRF'21, Int. Conf. on RF Superconductivity* (Geneva: JACoW Publishing) pp 105–8
[20] Inaba A 1980 *Jpn. J. Appl. Phys.* **19** 1553–9
[21] Bose S, Raychaudhuri P, Banerjee R, Vasa P and Ayyub P 2005 *Phys. Rev. Lett.* **95** 147003
[22] Fonnesu D *Doctoral Dissertation* University of Siegen submitted
[23] Ekin J W 2006 Properties of solids at low temperatures *Experimental Techniques for Low-Temperature Measurements* (Oxford: Oxford Academic) (https://doi.org/10.1093/acprof:oso/9780198570547.001.0001)
[24] Ohring M 2002 *Materials Science of Thin Films* (New York: Academic)
[25] Dhavale A S, Dhakal P, Polyanskii A A and Ciovati G 2012 *Supercond. Sci. Technol.* **25** 065014
[26] Robin A 2004 *J. Appl. Electrochem.* **34** 623–9